Title

A Cell Migration Tracking Tool Supports Coupling of Tissue Rotation to Elongation

Journal

Cell Reports, 21(3)

ISSN

2639-1856

Authors

Chen, Dong-Yuan
Crest, Justin
Bilder, David

Publication Date

2017-10-01

DOI

10.1016/j.celrep.2017.09.083

A novel cell migration tracking tool supports coupling of tissue rotation to elongation

Dong-Yuan Chen[1], Justin Crest[1] and David Bilder[1,2,*]

Affiliations:

[1]Department of Molecular and Cell Biology, University of California-Berkeley, Berkeley CA, 94720, USA

[2]Lead Contact

*Correspondence: bilder@berkeley.edu

SUMMARY

Cell migration is indispensable to morphogenesis and homeostasis. Live imaging allows mechanistic insights, but long-term observation can alter normal biology, and tools to track movements *in vivo* without perturbation are lacking. We develop here a tool called M-TRAIL, which reveals migration histories in fixed tissues. Using clones that overexpress GFP-tagged ECM components, motility trajectories are mapped based on durable traces deposited onto basement membrane. We applied M-TRAIL to Drosophila follicle rotation, comparing *in vivo* and *ex vivo* migratory dynamics. The rate, trajectory, and cessation of rotation in WT follicles measured *in vivo* and *ex vivo* were identical, as was rotation failure in *fat2* mutants. However, follicles carrying intracellularly truncated Fat2, previously reported to lack rotation *ex vivo*, in fact rotate *in vivo* at a reduced speed, thus revalidating the hypothesis that rotation is required for tissue elongation. The M-TRAIL approach could be applied to track and quantitate *in vivo* cell motility in other tissues and organisms.

INTRODUCTION

Cell migration is critical to metazoan biology. Developing organisms require massive morphogenetic movements to shape their organs, while tissues that encounter physical or chemical challenges induce cell motility during immune responses, wound healing and regenerative processes to maintain homeostasis. In cancer, cells' acquisition of the ability to migrate and metastasize is a hallmark of progression. To understand these fundamental biological processes, tools to accurately track and quantitate cell motility in tissues are crucial.

Tracing movements of individual or collectively migrating cells in non-transparent systems *in vivo* remains a challenge. Advances in *ex vivo* preparations, allowing an explanted tissue to be imaged for a period of hours, allow motility to be studied at cellular resolution (Shamir and Ewald, 2014). Nevertheless, few current techniques fully recapitulate development or homeostasis over long periods of time. Furthermore, imaging *per se* can lead to artifacts that may alter biological processes, via heat production, phototoxicity, and ROS generation (Liu et al., 2015). Overall, tools allowing long-term tracing of cell migration routes and velocities in intact but opaque organisms are highly limited.

One biological system that exemplifies the above is the *Drosophila* follicle (egg chamber). This epithelium-encased organ develops in the adult female abdomen, and undergoes a whole-tissue collective cell migration that spans several days (Bilder and Haigo, 2012; Cetera and Horne-Badovinac, 2015; Spradling, 1993). This migration leads to rotation of the entire organ through multiple rounds of revolution, and has been proposed to drive its elongation from spherical to ellipsoid (Haigo and Bilder, 2011). Because of its long-term nature and internal site, follicle rotation and its dynamics have only been imaged and quantified through explants in *ex vivo* culture. Whether the dynamics of cell migration differ *in vivo* remains unknown.

In this report, we develop a tool called M-TRAIL that allows unperturbed tracking of cell migration *in vivo*, and show its applicability in the follicle and other *Drosophila* tissues.

We further use M-TRAIL to critically evaluate results that have challenged the model coupling follicle rotation to elongation. We show that limitations of *ex vivo* culture account for the conflict, while the M-TRAIL-derived *in vivo* results are fully consistent with the model. These data demonstrate the value of M-TRAIL, which should be applicable to a range of other tissues and systems.

RESULTS

M-TRAIL as a tool to trace cell migrations *in vivo*

A valuable tool to track long-term cell migration *in vivo* would meet several criteria. First, it should minimally perturb normal physiology. Second, it should allow spatial mapping of past location at cellular resolution. Third, it should allow extraction of temporal information for quantifying migratory dynamics. We moved to develop such a tool, based on the interactions between cells and extracellular matrix (ECM). Cell-ECM interactions are central to migration, as cells in physiological conditions often crawl over an ECM substrate such as the basement membrane (BM); migrating cells can also remodel the local BM environment (Wolf and Friedl, 2011). On the timescale of most cell motility, BMs are relatively static and long lasting.

We exploited these properties in an approach called 'Matrix-labelling Technique for Real-time And Inferred Location (M-TRAIL)' (**Fig. 1A**). In M-TRAIL, migrating cells are engineered to inducibly and constitutively express tagged BM components. Following induction, these components will be secreted and deposited by the cell into the local BM. If an induced cell moves, a trail of relatively stable tagged ECM molecules will be deposited in the BM along the route of migration, and this durable trail can be imaged following fixation. Knowing the onset of BM component deposition allows one to infer average velocity as well as the trajectory of the migrating cell.

We tested whether the M-TRAIL concept could be successfully implemented, by exploring cell migrations in *Drosophila*. In this organism, stochastic single-cell expression clones can be generated using heat-induced FLP recombinase (hsFLP) to drive expression of a GAL4 gene separated from a constitutive promoter by cis-paired

FRT sites ('FLPout GAL4') (Blair, 2003). We paired *hsFLP* and *FLPout GAL4* transgenes with a UAS-driven, GFP-tagged version of one of the two *Drosophila* Collagen IV chains (GFP-Cg25c; Flybase: Col4a1), along with *UAS-Histone RFP* (**Fig. 1C**). Histone-RFP expression identifies the GAL4-expressing clone, although we noted that high levels of intracellular GFP-Cg25c puncta, presumably within the secretory system, were also sufficient.

We first applied M-TRAIL to motile cells in the follicle of *Drosophila* ovaries. In this organ, epithelial cells migrate collectively, circumferentially around the anterior-posterior axis, in a morphogenetic process known as follicle rotation (Haigo and Bilder, 2011). We heat-shocked females carrying M-TRAIL transgenes and then dissected, fixed, and examined ovaries 13 hours later. At 13 hour post heat shock (phs), a clear trail of GFP in the BM contiguous with the GAL4-expressing clone could be detected, extending in a single direction away from it in a swath extending around most of the circumferential axis (**Fig. 1B**). This is the axis in which follicle cells migrate in *ex vivo* preparations, and in which a previous BM-based *in vivo* assay inferred that migration occurs (Haigo and Bilder, 2011). Trails on the BM were not seen when clones expressed a soluble GFP-tagged secreted protein (preproANF-EMD) rather than GFP-Cg25c (**Fig. 1D**).

To determine when M-TRAILs could first be detected and how long they persisted, we examined follicles at various time points phs. In st. 8 follicles, which have been undergoing rotation for at least 36 hours, Cg25c-GFP was detected inside the clone at 6 hours phs, but no trails were visible (**Fig. 1E**). Trails were first detected at 7 hours phs, and increased in length as well as strength with time (**Fig. 1F, 1G**). Weak intracellular puncta and trails can be seen as early as st.5 follicles within an ovariole 17 hours phs (**Fig. 1H**). Trails were difficult to detect in st. 4 or earlier follicles, possibly because of the weak efficacy of the *act5c* promoter during these stages. We explored the stability of follicle M-TRAILs by examining ovarioles at 25 hours phs. Robust trails were detected in st. 10 follicles, which were likely at st. 6 when trail deposition began (**Fig. 1H)**. Overall, these results demonstrate the applicability of M-TRAIL to mapping cell migration.

Exploring criteria for M-TRAIL applicability

We evaluated the parameters within which M-TRAIL is useful for migration analysis by testing cells other than the follicle epithelium. The best-characterized motile cells in *Drosophila* are the border cells, a specialized subset of follicle cells that delaminate from the epithelium and migrate through the central germline towards the oocyte at st. 9 (Pocha and Montell, 2014). Interestingly, migrating border cells expressing M-TRAIL left only scant and transient trails along their route (**Fig. 2A and A'**). Since germ cells do not express BM components (**Fig. 2B, C),** this result suggests that a local BM may be necessary to provide a depot for the ECM components induced by M-TRAIL.

We then asked whether only cells that endogenously produce large amounts of BM components are suitable for M-TRAIL analysis. While follicle cells secrete Collagen IV into surrounding BM, imaginal disc epithelia instead construct their local BM predominantly from soluble Collagen IV synthesized by the fat body (Isabella and Horne-Badovinac, 2015a; Pastor-Pareja and Xu, 2011). We tested the ability of discs to secrete M-TRAIL-induced Cg25c-GFP. Staining for extracellular proteins revealed incorporation of disc cell-derived Cg25c-GFP into the local BM (**Fig. S1A**). Although cells in imaginal discs do not obviously migrate, the M-TRAIL approach appears applicable to cells that do not professionally secrete BM.

We turned to a third tissue to ask whether M-TRAIL might be used for tracking motility in cells outside of the ovary. *Drosophila* hemocytes are macrophage-like cells that undergo cell migration in response to tissue damage (Pastor-Pareja et al., 2008). We expressed GFP-Vkg specifically in hemocytes and then compared control imaginal discs to those that had been physically wounded *in situ*. Consistent with the documented production of basement membrane by hemocytes (Lunstrum et al., 1988), unwounded discs displayed a low level of GFP accumulation at their basal surface (**Fig. 2D**). In wounded discs, linear trails of basal GFP were often associated with hemocytes at the site of damage (**Fig. 2E**). These results suggest that M-TRAIL can be implemented in additional motile cell types.

Biogenesis, secretion, and incorporation of mature Collagen IV trimers into BM involves a specialized set of proteins, raising the question of whether alternative BM resident proteins might work more efficiently for M-TRAIL (Saito et al., 2009). We compared Cg25c-GFP to SPARC-HA, a tagged version of another secreted protein that is incorporated into the BM, by inducing M-TRAIL clones expressing both (Martinek et al., 2002). In follicles, SPARC-HA appeared to be more efficiently secreted than Cg25c-GFP, as less protein was detected intracellularly, but it appeared to diffuse more from the cell trajectory (**Fig. 2F**). However, SPARC overexpression can modify local BM properties and alter follicle shape (Isabella and Horne-Badovinac, 2015b). By contrast, Cg25c represents only one component of the obligate heterotrimeric Collagen IV, suggesting that its overexpression would not structurally alter the BM (Van De Bor et al., 2015). Consistent with this hypothesis, overexpression of Cg25c in the entire epithelia does not lead to any evident perturbation of morphogenesis (**Fig. S1B-D**).

M-TRAIL analysis of WT follicle morphogenesis *in vivo*

Having established the general utility of M-TRAIL, we applied it to analyze follicle rotation in more detail, comparing the *in vivo* data to that inferred from other approaches. Rotation has previously been analyzed using *ex vivo* live imaging, from which linear and angular velocities (ω) have been measured (Cetera et al., 2014; D.-Y. Chen et al., 2016; X. J. Chen et al., 2014; Haigo and Bilder, 2011; Viktorinová and Dahmann, 2013). Current *ex vivo* culture protocols support follicle viability for a maximum of ~10 hours, representing only a fraction of the 42 hours through which rotation is thought to occur *in vivo*. We used M-TRAIL to compare *in vivo* rotation velocities and those *ex vivo*, analyzing the length of trails in fixed M-TRAIL-induced st. 8 follicles 9 hours phs by using the 'unrolling' algorithm lmSAnE (D.-Y. Chen et al., 2016) (**Fig. 3A-C**). Accounting for the 7 hour onset time of M-TRAIL induction, at st.8 *in vivo* ω equals 50º/hr, very similar to that measured *ex vivo* (**Fig. 3D**). These results demonstrate that in WT follicles, short-term *ex vivo* conditions recapitulate the speed of cell motility *in vivo.*

In addition to rotation from st. 2 to 8, follicles undergo a morphogenetic event variously termed 'posterior migration' or 'anterior accommodation' from st. 9 to 10, after rotation ceases (Kolahi et al., 2009; Spradling, 1993). During this process, the anterior follicle

epithelium undergoes rapid reorganization: cells alter their morphology from cuboidal to squamous and concurrently elongate anisotropically towards the anterior pole (Brigaud et al., 2015). Interestingly, M-TRAIL captured this movement: in trails initiating at late st. 7, both cessation of rotation and a posteriorly-directed shift were seen in the squamous 'stretch' cells at the anterior, while only the former process was seen in the columnar cells at the posterior (**Fig. 3E**). This result confirms that the anterior 'stretch' cells change their position relative to the BM, while posterior cells are relatively static. Moreover, the lengthy (>24 hour) time courses that capture complete rotations as well as anterior morphogenesis (**Fig. 3F**) far exceed the limits of follicle viability under current *ex vivo* culture conditions; M-TRAIL uniquely allows their visualization.

M-TRAIL analysis of *fat2* mutant follicles

As M-TRAIL can be used to study WT follicle development, we then turned to mutant analysis. The most dramatic perturbation of follicle cell migration occurs in flies mutant for *fat2*, which encodes an atypical cadherin implicated in planar polarity and symmetry-breaking (D.-Y. Chen et al., 2016; Viktorinova et al., 2009). In *fat2* null follicles, rotation *ex vivo* completely fails, never initiating at st. 2 and not measurably moving throughout st. 8 (Cetera et al., 2014; D.-Y. Chen et al., 2016; Viktorinová and Dahmann, 2013). We tested whether the *ex vivo* results accurately reflect the *in vivo* situation by inducing M-TRAIL in *fat2* null follicles. *Fat2* follicles produced ectopic Cg25c-GFP and deposited it into the BM comparable to WT. However, M-TRAIL clones induced either at st. 5-6 or st. 7-8 did not produce a measurable circumferential trail, even 17 hours phs (**Fig. 4A, B**). Importantly, posteriorly-directed trails in stretch cells at st. 9 were visible (**Fig. S2A**), consistent with the observation that acquisition of squamous morphology and anterior follicle morphogenesis are undisturbed by *fat2* mutation.

Thus, the lack of circumferential M-TRAILs in *fat2* mutants rigorously establishes the absence of rotation *in vivo*, as previously seen *ex vivo*.

Follicles lacking the Fat2 intracellular region rotate *in vivo*

A recent paper interrogated the role of *fat2* in rotation and elongation by designing and testing novel alleles, carried on fosmids in a *fat2* null mutant background (Aurich and Dahmann, 2016). These authors found that deletion of either the intracellular region (ΔICR) alone or the transmembrane domain in conjunction with the ICR (ΔTMICR) prevented rotation *ex vivo*. Interestingly, follicles lacking ICR alone (*fat2ΔICR*) were able to elongate appropriately and achieve late-stage PCP cytoskeletal organization, despite their observed lack of PCP rotation. The authors proposed that this genotype, which apparently uncouples the two processes, demonstrates that PCP rotation is not required for follicle elongation and PCP morphogenesis.

We investigated this proposition using M-TRAIL to analyze rotation of the new *fat2* alleles *in vivo*. We first confirmed that *fat2ΔICR* follicles elongate normally but fail to rotate *ex vivo* **(Fig. S2B-E)**. As previously reported, no circumferential rotation could be detected under *ex vivo* live imaging during a 2 hour course; in this *fat2ΔICR* follicles resembled *fat2* nulls (**Fig. S2B**). Surprisingly, when we utilized M-TRAIL to visualize *in vivo* migration, clear circumferentially oriented trails were visible in *fat2ΔICR* follicles but not *fat2* null nor *fat2ΔTMICR* 13 hours phs (**Fig. 4B, C, and D**). Interestingly, trails appeared shorter than those seen in WT follicles (**Fig. 4A**). We therefore tested if *fat2ΔICR*-carrying follicles have altered rotation dynamics by directly comparing them with heterozygous sibling follicles under the same M-TRAIL induction conditions (**Fig. 4E)**. While st.8 follicles carrying either a WT *fat2* allele or a functional *fat2-GFP* fosmid have ω=44º/hr, follicles carrying only *fat2ΔICR* were ~50% slower, with ω=25º/hr. We confirmed these results using a second *fat2* mutant background (**Fig. S2F**). This result demonstrates that *fat2ΔICR* follicles indeed rotate *in vivo*, although an undefined limitation of current culture conditions does not support *ex vivo* rotation. Importantly, it further establishes that this genotype does not in fact uncouple rotation from elongation.

Slow-rotating *fat2ΔICR* follicles have functionally softer but anisotropic BMs

Does the normal elongation of *fat2ΔICR* follicles establish that even a low rate of PCP follicle rotation is sufficient to generate the tissue organization and mechanical properties required for appropriate morphogenesis? We have recently shown that follicle shape is determined by mechanical properties provided by its fibril-like BM, with

key parameters including BM PCP organization and A-P patterned levels (Crest et al., 2017). We analyzed both parameters in *fat2ΔICR* follicles with ImSAnE. In agreement with previous data, *fat2ΔICR* follicles generate PCP Collagen IV fibrils but these fibrils are shorter as well as less dense than those seen in WT (**Fig. 5A-D**) (Aurich and Dahmann, 2016). However, the anisotropic A-P expression gradient of Collagen IV resembled WT (**Fig. 5E-F**). The mechanical stiffness of the *fat2ΔICR* follicle BM was then tested, using both Atomic Force Microscopy (AFM) along the A-P and circumferential axes (**Fig. 5G)** and an osmotic swelling assay in which follicles are placed in distilled water (**Fig. 5H)**. We have previously used these techniques to show that WT follicles display an anisotropic A-P stiffness gradient that directs elongation (Crest et al., 2017). AFM analysis on *fat2ΔICR* follicle BM showed the existence of an anisotropic A-P stiffness gradient, but revealed that it appears softer than WT (**Fig. 5I**). Indeed, when challenged with osmotic stress, *fat2ΔICR* follicles burst more frequently than WT (**Fig. 5J**). Nevertheless, bursting is restricted to poles (**Fig. 5K**), consistent with the anisotropic stiffness measurements. Thus, reduced fibril formation and a softer BM correlate with the slower albeit normally-oriented tissue rotation revealed by M-TRAIL. Overall, the results are consistent with the model that a degree of PCP migration of the follicle epithelium, generating PCP fibrils and consistent circumferential stiffness, is indeed essential for appropriate organ elongation.

DISCUSSION

M-TRAIL tracking of cell migration *in vivo*

Ex vivo live imaging has led to important discoveries about cell motility during development and homeostasis. Whether explant culture systems fully recapitulate *in vivo* biology, however, remains an issue, especially for biological processes that span longer time scales. Here we provide a tool to track long-term cell motility *in vivo,* by quantitating ECM traces stably deposited by migrating cells. The genesis of this strategy lies in a previous experiment in the *Drosophila* follicle, where large clones endogenously expressing tagged Collagen IV were marked by mitotic recombination *in trans* and used to demonstrate that follicle rotation organizes BM *in vivo* (Haigo and

Bilder, 2011). M-TRAIL uses *cis*-recombination to allow temporal control over ECM component secretion, as well as to free induction from cell division, and can be utilized even in natively non-ECM-producing cells. Importantly, the ability to generate single cell clones allows cellular resolution of migratory tracks. Overall, M-TRAIL enables long-term, quantitative measurements of cell migration in fixed tissues and can potentially track other cellular dynamics, such as cell division and rearrangements, under physiological conditions.

Several points are relevant to applying and interpreting M-TRAIL. First, cells must be able to secrete the M-TRAIL protein. Export of Collagen chains, including Collagen IV, can involve specialized machinery that may not be active in all cells (Saito et al., 2009). In our experiments, an alternative ECM protein, SPARC, was more efficiently secreted, but appeared to diffuse farther and also has the ability to alter ECM stiffness. Inactive mutant forms of SPARC or other ECM proteins may be appealing directions for future refinements (Morrissey et al., 2016). Second, M-TRAIL depends on the pre-existence and stability of the BM. In early animals, there may be insufficient BM for incorporation, and throughout development there are migrations that do not involve integrin-ECM interactions (Paluch et al., 2016). Moreover, trail stability is subject to BM remodeling, such as degradation by matrix metalloproteases. BMs can also be more dynamic than commonly appreciated (Loganathan et al., 2016; Morrissey and Sherwood, 2015); this should be considered when plotting speed and trajectory of the source cell relative to the BM and the rest of the organism. Third, it is necessary to determine the lag time to trail detection in the cells under analysis. This includes not just genetic induction but also microscopic visualization. Since the amount of ECM protein deposited will correlate with the cellular ‘dwell time’ over a region of BM, rapid migrations as well as those that occur over short periods of time will require more sensitive detection. Improved secretion, brighter fluorophores, and multiple epitope tags can benefit this. While we have demonstrated M-TRAIL’s value in *Drosophila*, the relationship of migrating cells to the ECM is conserved throughout metazoans (Brown, 2011), so M-TRAIL should be useful for a wide variety of biological systems.

Coupling of follicle elongation to tissue rotation

The original discovery of tissue rotation in WT follicles, and its failure in non-elongating mutants, led to the proposal that rotation is required for elongation, by creating PCP organization of cytoskeletal and BM elements to form the previously hypothesized 'molecular corset' (Gutzeit et al., 1991; Haigo and Bilder, 2011). This initial model has guided numerous subsequent studies, whose data are largely consistent with its formulation. The recent report that *fat2ΔICR* follicles uncouple rotation and elongation thus presents an important challenge to the model (Aurich and Dahmann, 2016). Here we resolve this discrepancy by showing that *fat2ΔICR* follicles indeed rotate *in vivo*, although they do not in *ex vivo* culture for reasons currently unknown. At this time, we are unaware of any non-rotating follicle genotype that is capable of elongation, consistent with the proposition that rotation is a morphogenetic mechanism that generates the mechanical environment necessary to shape the *Drosophila* egg.

Importantly, although *fat2ΔICR* follicles show appropriate aspect ratios, they are not fully normal in several parameters. Migration is slowed, the BM fibrils that are produced are attenuated, and the result is a functionally softer BM than in WT follicles. Although these phenotypes could point to a direct role of the *fat2ΔICR* in BM secretion, an attractive alternative hypothesis is that they instead reflect a role for tissue rotation rates in constructing BM networks and their mechanical properties. Integrin-mediated traction forces are known to drive a positive feedback loop linking ECM stiffness to cell migration speeds in many systems (Parsons et al., 2010); this conserved molecular mechanism, amplified by the continuous topology of the follicles' axis of rotation, could drive the construction of a robust BM that instructs elongation.

The demonstration that *fat2ΔICR* follicles undergo PCP cell migration sheds further light on the activity of Fat2 itself. Fat2 shows PCP localization in rotating follicles and binds to actin polymerization-stimulating WAVE complex proteins; both of these properties are mediated by the ICR (Barlan et al., 2017; Squarr et al., 2016; Viktorinová and Dahmann, 2013). The ability of follicles lacking the Fat2 ICR to rotate demonstrates that a direct Fat2-WRC interaction is not essential for collective cell motility, placing more emphasis

on the Fat2 extracellular domain, perhaps in a ligand-like role (see also (Barlan et al., 2017)). This ability also emphasizes that it is PCP rotation, rather than Fat2 localization, that is correlated with proper organization of cytoskeleton and ECM components. Recent work identifies an initial and essential requirement for Fat2 in regulating symmetry-breaking microtubule polarity in the germarium, in a manner independent of actin organization (D.-Y. Chen et al., 2016). The localization of Fat2 during these stages is not known but the ability of *fat2ΔICR* follicles to break chiral symmetry is consistent with an ECD-mediated role. In general, the use of M-TRAIL to both reveal unexpected migration and quantitate its rate in this genotype, as well as in future manipulations, will guide testable hypotheses for mechanisms that couple rotation of a tissue to the mechanical properties that drive its elongation.

While M-TRAIL uncovered one limitation of *ex vivo* follicle imaging, reconciling contradictory results, it is important to emphasize that in other aspects it was concordant with prior analyses. In particular, the migration rate, trajectory, and cessation of rotation in WT follicles measured *in vivo* by M-TRAIL were identical to those observed *ex vivo,* as was the failure of rotation in *fat2* mutants. This validates the general *ex vivo* approach to study follicle rotation, but points out that live imaging of some mutant genotypes may not accurately reflect what occurs in the animal. The creation of more genetically convenient as well as more sensitive M-TRAIL variants will expand the range of situations in which this new tool can be used.

EXPERIMENTAL PROCEDURES

All fluorescent images were acquired on a Zeiss LSM700 confocal microscope. M-TRAIL follicle clones were induced by 15 or 20 minute heat shocks of 3-day old, fed adult females in a 37ºC water bath. Ovaries were dissected and stained after hours post heat shock (phs) indicated on the figures. Over 50% follicles show multiple single clones along the A-P arc and ~10% have non-overlapping single clones. Non-permeablized immunostains were performed without detergent. ImSAnE unrolling and analyses were executed as previously described on full stacks of confocal sections of follicles stained with Alexa Fluor647-conjugated phalloidin (D.-Y. Chen et al., 2016). The phalloidin channel was used to generate point clouds for unrolling. Conditions for *ex vivo* follicle culture were as previously described (D.-Y. Chen et al., 2016). AFM

measurements, bursting assays, and Collagen IV-GFP fibril intensity measurements were done as described (Crest et al., 2017). Fibril density and length were measured as in (Isabella and Horne-Badovinac, 2015b) on the central region of ImSAnE-flattened images. Error bars in charts represents SEM and statistical significance was assessed by Welch's unequal variances *t*-test. Additional details are described in **Supplemental Experimental Procedures**.

AUTHOR CONTRIBUTIONS

D.Y.C. and J.D. conducted the experiments; D.Y.C and D.B. designed the experiments and wrote the paper.

ACKNOWLEDGMENTS

We thank Christian Dahmann, Stephane Noselli, Eduardo Moreno, Katja Brückner, Iswar Hariharan, and the Bloomington Stock Center for sending reagents, Geert de Vreede for assistance in discs wounding experiments, and are grateful to the Bilder lab for helpful discussions. This work was supported by NIH RO1s GM068675 and GM111111.

REFERENCES

Aurich, F., Dahmann, C., 2016. A Mutation in fat2 Uncouples Tissue Elongation from Global Tissue Rotation. Cell Reports. doi:10.1016/j.celrep.2016.02.044

Barlan, K., Cetera, M., Horne-Badovinac, S., 2017. Fat2 and Lar Define a Basally Localized Planar Signaling System Controlling Collective Cell Migration. Dev Cell 40, 467–477.e5. doi:10.1016/j.devcel.2017.02.003

Bilder, D., Haigo, S.L., 2012. Expanding the morphogenetic repertoire: perspectives from the Drosophila egg. Dev Cell 22, 12–23. doi:10.1016/j.devcel.2011.12.003

Blair, S.S., 2003. Genetic mosaic techniques for studying Drosophila development. Development 130, 5065–5072. doi:10.1242/dev.00774

Brigaud, I., Duteyrat, J.-L., Chlasta, J., Le Bail, S., Couderc, J.-L., Grammont, M., 2015. Transforming Growth Factor β/activin signalling induces epithelial cell flattening during Drosophila oogenesis. Biology Open 4.

Brown, N.H., 2011. Extracellular matrix in development: insights from mechanisms conserved between invertebrates and vertebrates. Csh Perspect Biol 3. doi:10.1101/cshperspect.a005082

Cetera, M., Horne-Badovinac, S., 2015. Round and round gets you somewhere: collective cell migration and planar polarity in elongating Drosophila egg chambers. Curr. Opin. Genet. Dev. 32, 10–15. doi:10.1016/j.gde.2015.01.003

Cetera, M., Ramirez-San Juan, G.R., Oakes, P.W., Lewellyn, L., Fairchild, M.J., Tanentzapf, G., Gardel, M.L., Horne-Badovinac, S., 2014. Epithelial rotation

promotes the global alignment of contractile actin bundles during Drosophila egg chamber elongation. Nature Communications 5, 5511. doi:10.1038/ncomms6511
Chen, D.-Y., Lipari, K.R., Dehghan, Y., Streichan, S.J., Bilder, D., 2016. Symmetry Breaking in an Edgeless Epithelium by Fat2-Regulated Microtubule Polarity. Cell Reports 15, 1125–1133. doi:10.1016/j.celrep.2016.04.014
Chen, X.J., Squarr, A.J., Stephan, R., Chen, B., Higgins, T.E., Barry, D.J., Martin, M.C., Rosen, M.K., Bogdan, S., Way, M., 2014. Ena/VASP proteins cooperate with the WAVE complex to regulate the actin cytoskeleton. Dev Cell 30, 569–584. doi:10.1016/j.devcel.2014.08.001
Crest, J., Diz-Munoz, A., Chen, D.-Y., Fletcher, D.A., Bilder, D., 2017. Organ sculpting by patterned extracellular matrix stiffness. eLife 6, e24958. doi:10.7554/eLife.24958
Gutzeit, H.O., Eberhardt, W., Gratwohl, E., 1991. Laminin and basement membrane-associated microfilaments in wild-type and mutant Drosophila ovarian follicles. journal of cell Science 100 (Pt 4), 781–788.
Haigo, S.L., Bilder, D., 2011. Global tissue revolutions in a morphogenetic movement controlling elongation. Science 331, 1071–1074. doi:10.1126/science.1199424
Isabella, A.J., Horne-Badovinac, S., 2015a. Building from the Ground up: Basement Membranes in Drosophila Development. Current Topics in Membranes 76, 305–337.
Isabella, A.J., Horne-Badovinac, S., 2015b. Dynamic regulation of basement membrane protein levels promotes egg chamber elongation in Drosophila. Dev Biol. doi:10.1016/j.ydbio.2015.08.018
Kolahi, K.S., White, P.F., Shreter, D.M., Classen, A.K., Bilder, D., Mofrad, M.R., 2009. Quantitative analysis of epithelial morphogenesis in Drosophila oogenesis: New insights based on morphometric analysis and mechanical modeling. Dev. Biol. 331, 129–139. doi:10.1016/j.ydbio.2009.04.028
Liu, Z., Lavis, L.D., Betzig, E., 2015. Imaging live-cell dynamics and structure at the single-molecule level. Mol. Cell 58, 644–659. doi:10.1016/j.molcel.2015.02.033
Loganathan, R., Rongish, B.J., Smith, C.M., Filla, M.B., Czirok, A., Bénazéraf, B., Little, C.D., 2016. Extracellular matrix motion and early morphogenesis. Development 143, 2056–2065. doi:10.1242/dev.127886
Lunstrum, G.P., Bachinger, H.-P., Fessler, L.I., Duncan, K.G., Nelson, R.E., Fessler, J.H., 1988. Drosophila basement membrane procollagen IV. I. Protein characterization and distribution. J. Biol. Chem. 263, 18318–18327.
Martinek, N., Zou, R., Berg, M., Sodek, J., Ringuette, M., 2002. Evolutionary conservation and association of SPARC with the basal lamina in Drosophila. Dev Genes Evol 212, 124–133.
Morrissey, M.A., Jayadev, R., Miley, G.R., Blebea, C.A., Chi, Q., Ihara, S., Sherwood, D.R., 2016. SPARC Promotes Cell Invasion In Vivo by Decreasing Type IV Collagen Levels in the Basement Membrane. PLoS Genet. 12, e1005905. doi:10.1371/journal.pgen.1005905
Morrissey, M.A., Sherwood, D.R., 2015. An active role for basement membrane assembly and modification in tissue sculpting. journal of cell Science 128, 1661–1668. doi:10.1242/jcs.168021
Paluch, E.K., Aspalter, I.M., Sixt, M., 2016. Focal Adhesion-Independent Cell Migration. Annu. Rev. Cell Dev. Biol. 32, 469–490. doi:10.1146/annurev-cellbio-111315-125341

Parsons, J.T., Horwitz, A.R., Schwartz, M.A., 2010. Cell adhesion: integrating cytoskeletal dynamics and cellular tension. Nature Reviews Molecular Cell Biology 11, 633–643. doi:10.1038/nrm2957
Pastor-Pareja, J.C., Wu, M., Xu, T., 2008. An innate immune response of blood cells to tumors and tissue damage in Drosophila. Dis Model Mech 1, 144–154. doi:10.1242/dmm.000950
Pastor-Pareja, J.C., Xu, T., 2011. Shaping cells and organs in Drosophila by opposing roles of fat body-secreted Collagen IV and perlecan. Dev Cell 21, 245–256. doi:10.1016/j.devcel.2011.06.026
Pocha, S.M., Montell, D.J., 2014. Cellular and molecular mechanisms of single and collective cell migrations in Drosophila: themes and variations. Annu. Rev. Genet. 48, 295–318. doi:10.1146/annurev-genet-120213-092218
Saito, K., Chen, M., Bard, F., Chen, S., Zhou, H., Woodley, D., Polischuk, R., Schekman, R., Malhotra, V., 2009. TANGO1 facilitates cargo loading at endoplasmic reticulum exit sites. Cell 136, 891–902. doi:10.1016/j.cell.2008.12.025
Shamir, E.R., Ewald, A.J., 2014. Three-dimensional organotypic culture: experimental models of mammalian biology and disease. Nature Reviews Molecular Cell Biology 15, 647–664. doi:10.1038/nrm3873
Spradling, A.C., 1993. Developmental genetics of oogenesis., in: Bate, M., Martinez Arias, A. (Eds.), The Development of Drosophila Melanogaster. CSHL Press, New York, pp. 1–70.
Squarr, A.J., Brinkmann, K., Chen, B., Steinbacher, T., Ebnet, K., Rosen, M.K., Bogdan, S., 2016. Fat2 acts through the WAVE regulatory complex to drive collective cell migration during tissue rotation. J. Cell Biol. 212, 591–603.
Van De Bor, V., Zimniak, G., Papone, L., Cerezo, D., Malbouyres, M., Juan, T., Ruggiero, F., Noselli, S., 2015. Companion Blood Cells Control Ovarian Stem Cell Niche Microenvironment and Homeostasis. Cell Reports 13, 546–560. doi:10.1016/j.celrep.2015.09.008
Viktorinova, I., Konig, T., Schlichting, K., Dahmann, C., 2009. The cadherin Fat2 is required for planar cell polarity in the Drosophila ovary. Development 136, 4123–4132. doi:10.1242/dev.039099
Viktorinová, I., Dahmann, C., 2013. Microtubule polarity predicts direction of egg chamber rotation in Drosophila. Current Biology 23, 1472–1477. doi:10.1016/j.cub.2013.06.014
Wolf, K., Friedl, P., 2011. Extracellular matrix determinants of proteolytic and non-proteolytic cell migration. Trends Cell Biol. 21, 736–744. doi:10.1016/j.tcb.2011.09.006

FIGURE LEGENDS

Figure 1. M-TRAIL, a novel tool to track cell migration *in vivo*.

(A) Schematic of M-TRAIL strategy. A one-cell clone (red) overexpressing a tagged ECM protein (green) is generated through genetic mosaic techniques. Secreted ECM protein is deposited in local BM, leaving a trail if the cell migrates before fixation.

(B) Implementation of M-TRAIL. Early st. 9 follicle with M-TRAIL induced, 13 hrs phs. Single epithelial clones reveal trajectory of cell migration during follicle rotation. 'Anti-GFP' here and below indicates that anti-GFP immunohistochemistry was performed without cell permeabilization. Left panel shows maximum Z projection of confocal stacks. Right panels show rotated views of opacity projection. Scale bar:10 μm.

(C) Genetic components used to generate M-TRAIL in **Figs. 1-5**. A heat shock-inducible recombinase causes excision of a stop cassette to initiate GAL4 production. GAL4 in turn drives expression of a nuclear RFP and GFP-tagged chain of Collagen IV.

(D) Early st. 9 follicle with non-ECM secreted protein tagged with GFP, 12 hrs phs. No trails are seen.

(E, F) Intracellular GFP-Cg25c can be detected 6 hrs phs, but trails are not evident until 7-8 hrs phs.

(G) Quantitation of M-TRAIL length, measured by percent of follicle circumference. Data are represented as mean +/- SEM.

(H, I) Trails can be seen in follicles from st. 5 to st. 10.

Figure 2. Criteria for M-TRAIL application

(A) In contrast to follicle epithelial cells, migrating border cells expressing GFP-Cg25c do not leave trails.

(B, C) Germline cells lack expression of BM components Vkg and Perlecan.

(D) In larvae expressing GFP-Vkg in hemocytes, unwounded wing imaginal discs (expressing a red fluorophore in the pouch) show only low-level GFP signal in the BM.

(E) 7 hours following wounding, hemocytes (arrowhead) adhere close to wound sites (white dotted line) and are often found next to BM trails of GFP (grey arrow).

(F) The ECM protein SPARC-HA can be used in M-TRAIL, although it diffuses farther from cells than GFP-Cg25c.

Figure 3. Characterization of follicle morphogenesis *in vivo* using M-TRAIL

(A) Use of ImSAnE 'flattening' algorithm to project 3D follicle epithelium onto 2D plane.

(B, C) Flattened trails present in M-TRAIL follicles cultured for 2 hrs *in vivo* vs *ex vivo.*

(D) Rotational angular velocity (ω, calculated by trail length as a fraction of follicle circumference) reveals no difference *ex vivo* vs *in vivo*. Data are represented as mean +/- SEM.

(E) Anterior clones (arrow) leave trails that are circumferential during st. 7-8, but then shift toward the posterior after rotation ceases at st. 9. Posterior clones (arrowhead) show rotation but no A-P shift.

(F) St. 9 follicle with two clones showing long term tracing. Note the complete rotations evident; also note the greater posterior shift in the more anterior clone.

Figure 4. *fat2ΔICR* follicles rotate *in vivo,* albeit at a slower rate

(A-D) Maximum intensity Z and ImSAnE-flattened projections of M-TRAIL induced follicles carrying different *fat2* alleles. **(A)** Follicles carrying a WT allele generate long trails; **(B)** homozygous *fat2* follicles show no trails; **(C)** follicles carrying *fat2ΔICR* show short trails; **(D)** follicles carrying *fat2ΔTMICR* show no trails.

(E) Angular velocity calculated by trail length; *fat2ΔICR* follicles rotate at 57% the rate of those carrying a WT allele, while *fat2ΔTMICR* do not rotate at all. Data are represented as mean +/- SEM.

Figure 5. *fat2ΔICR* follicles show altered mechanical properties

(A-B) Confocal projections of Collagen IV-GFP in WT and *fat2ΔICR* follicles.

(C-D) Collagen IV fibril analysis quantitates shorter and less dense fibrils in *fat2ΔICR* vs control (*fat2* heterozygous) follicles. Data are represented as mean +/- SEM.

(E-F) Anisotropic A-P distributions of Collagen IV-GFP are similar between the two genotypes.

(G) Schematic of Atomic Force Microscopy experiments. Follicles are probed at different regions along the A-P axis to measure BM (green) stiffness.

(H) Schematic of bursting assay. Follicles are placed in distilled water to swell tissue; timing and position of BM (green) rupture reflects BM mechanics.

(I) AFM measurements reveal that *fat2ΔICR* follicles maintain an AP stiffness gradient similar to WT, but display modest softening. Data are represented as mean +/- SEM.

(J) Following osmotic challenge, *fat2ΔICR* follicles burst more frequently than WT follicles, but less frequently than *fat2ΔTMICR* follicles. Data are represented as mean +/- SEM.

(K) Like WT, bursting in *fat2ΔICR* follicles does not occur in the central region, in contrast to *fat2ΔTMICR* follicles.

Figure 1

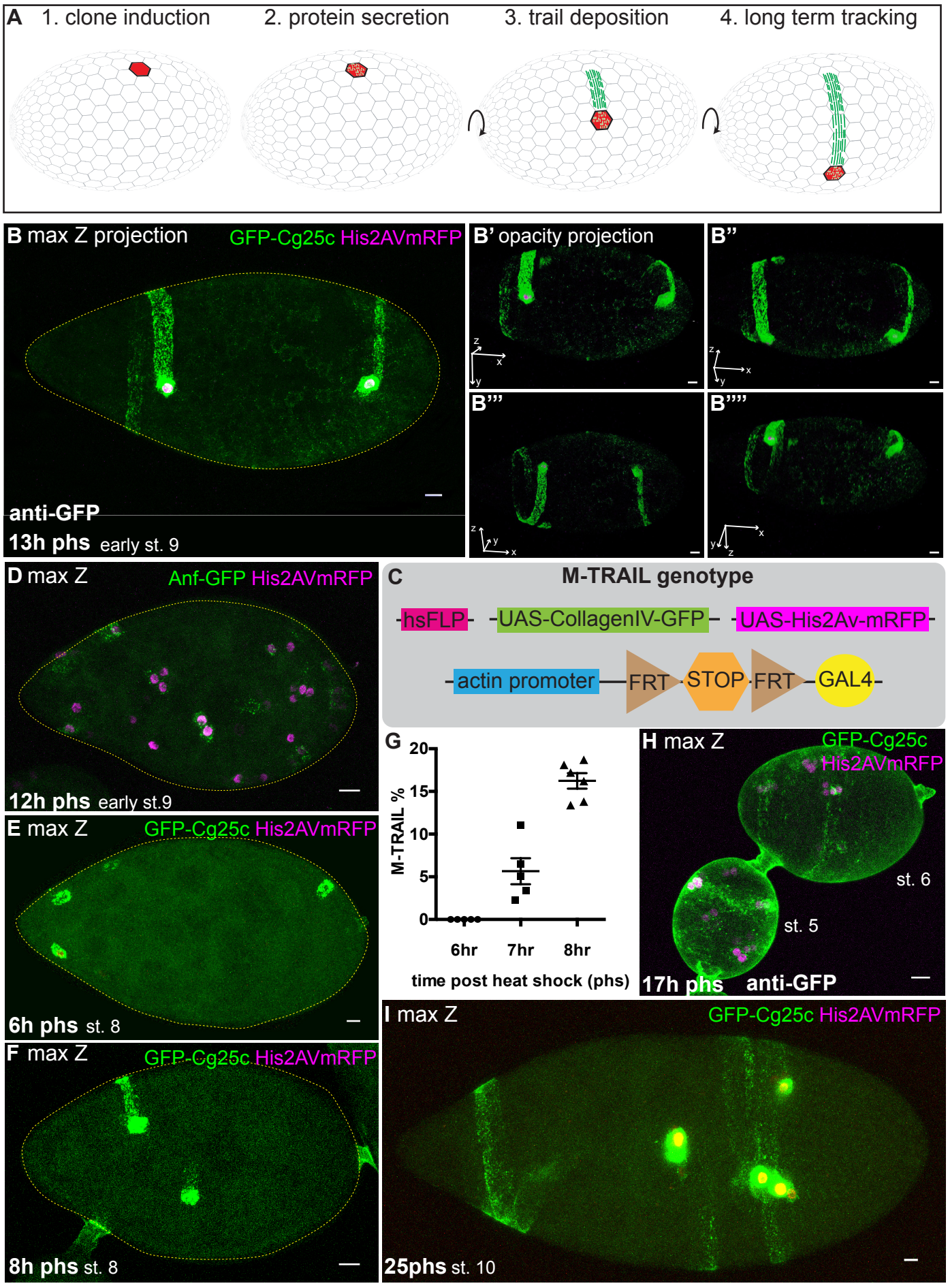

Fig.1

Figure 2

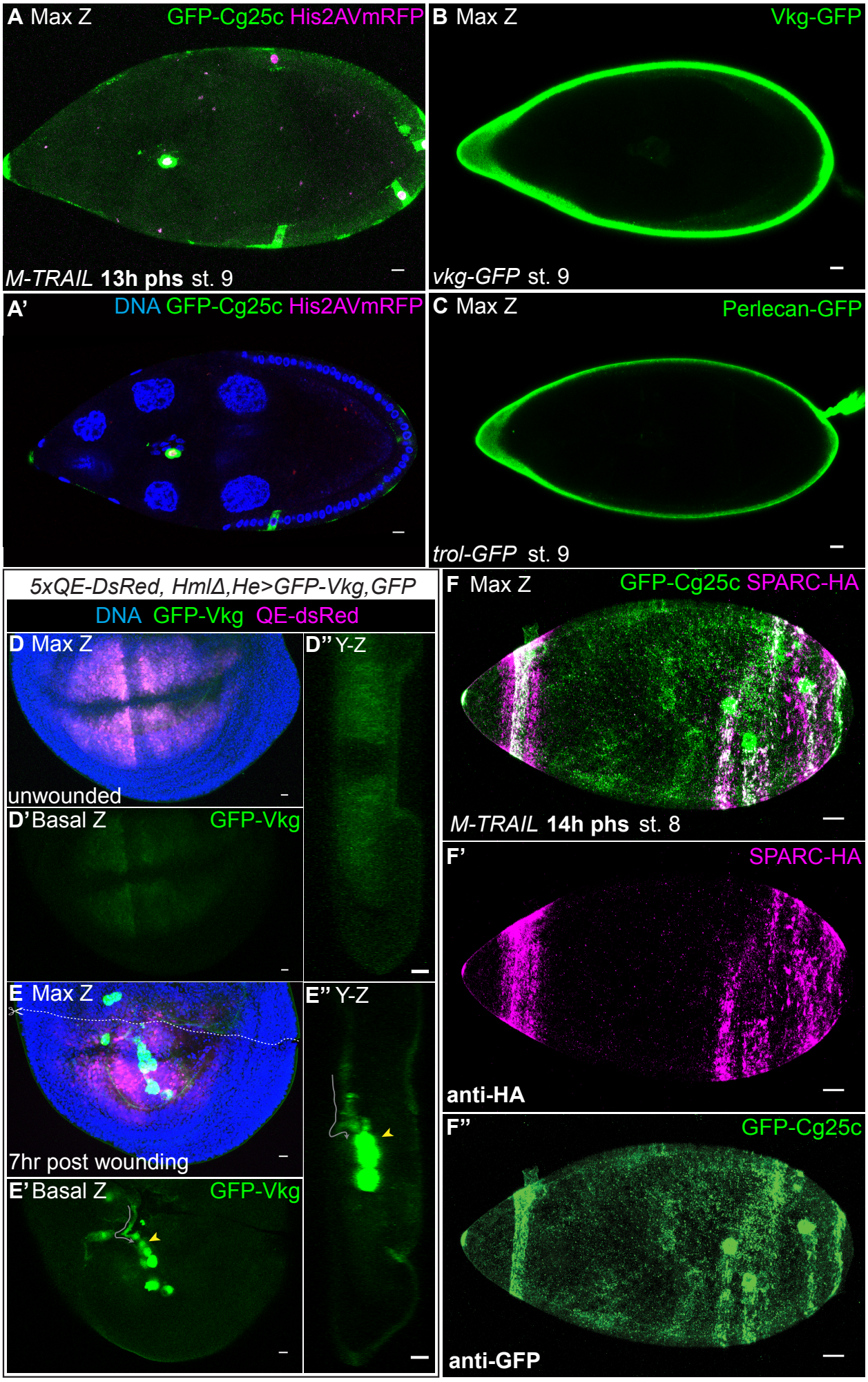

Fig.2

Figure 3

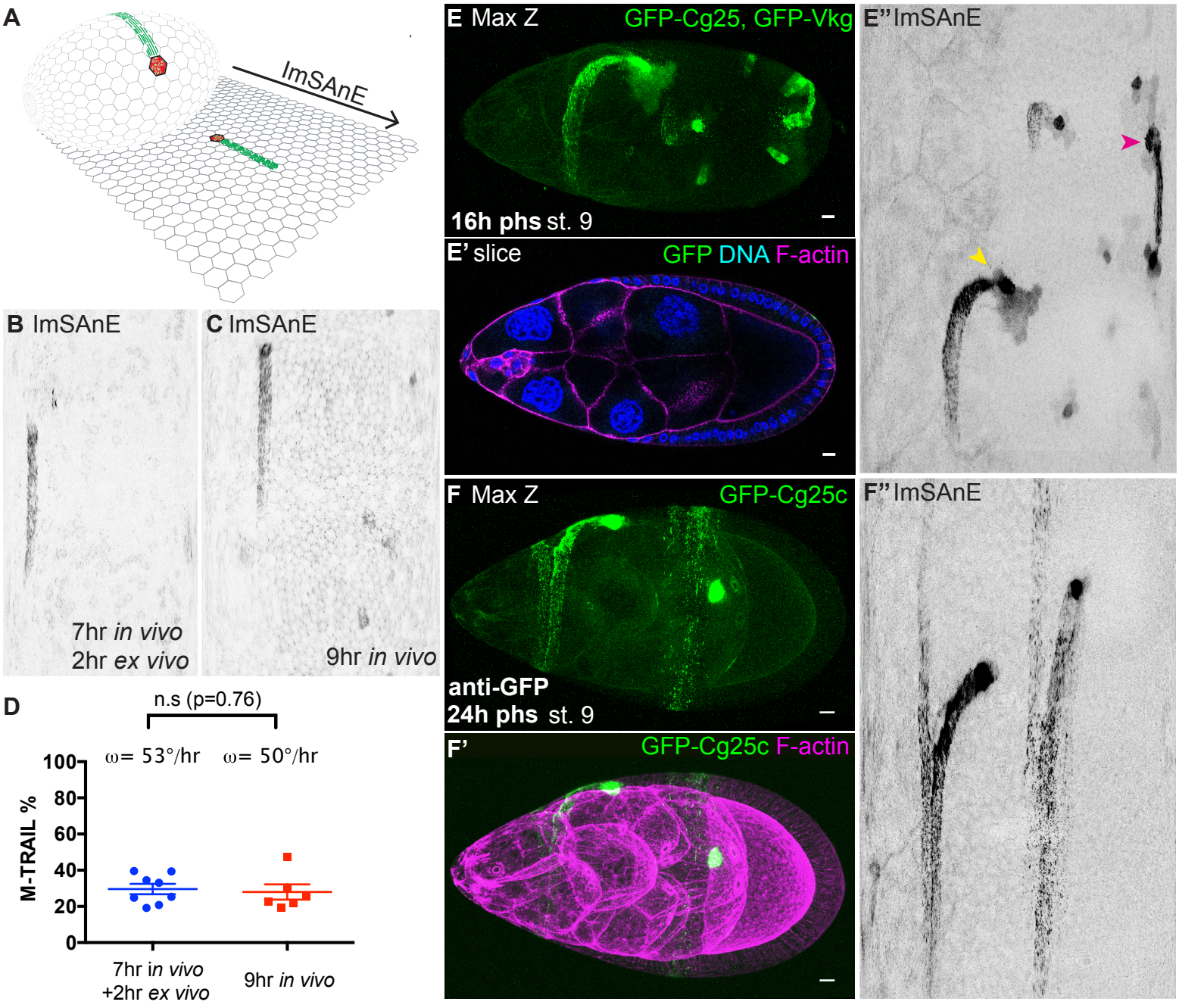

Fig.3

Figure 4

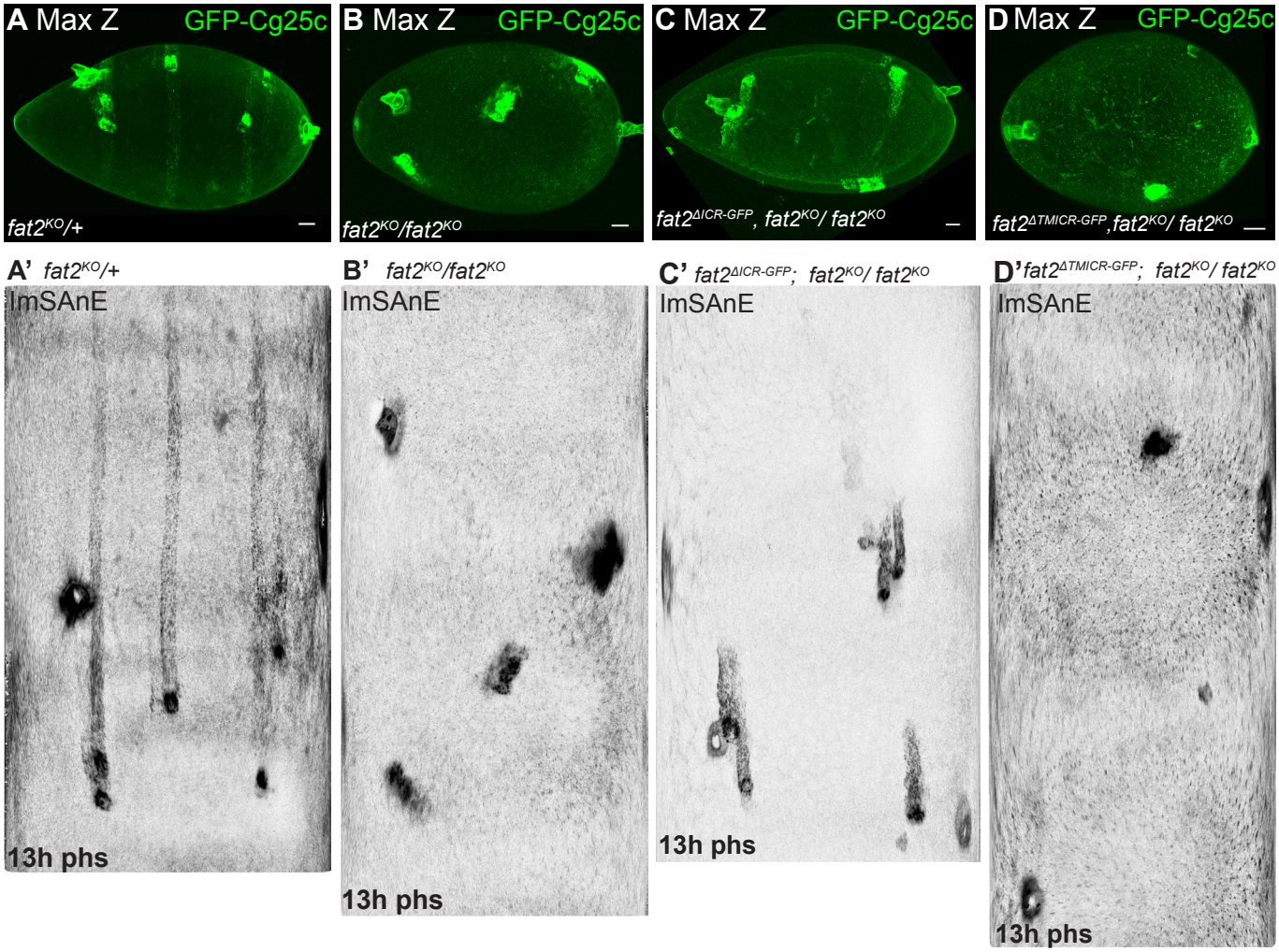

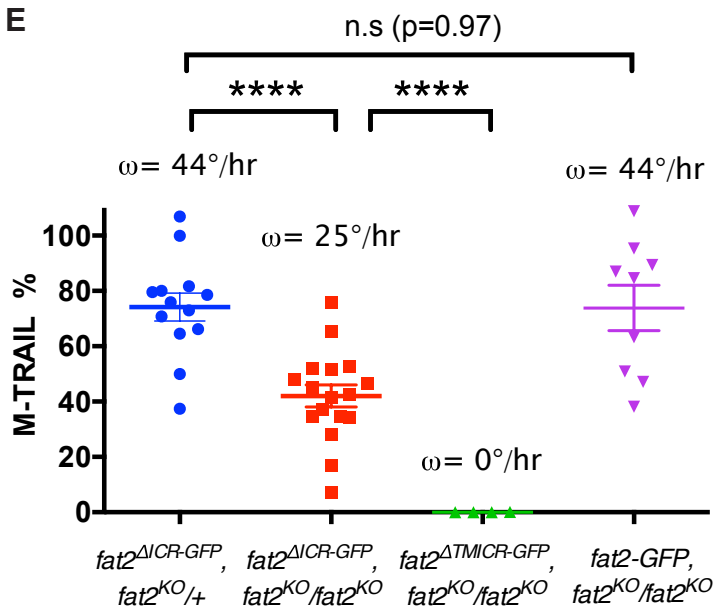

Fig.4

Figure 5

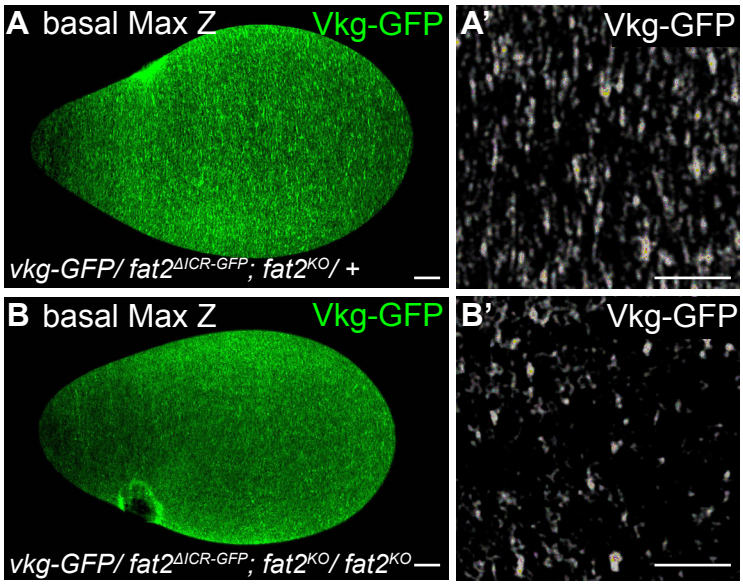

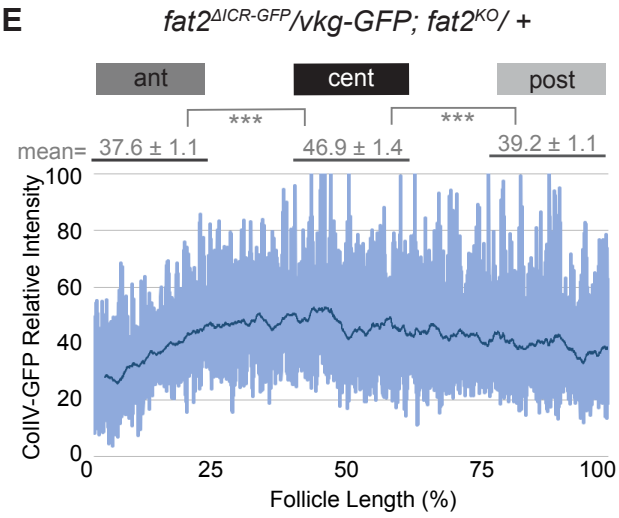

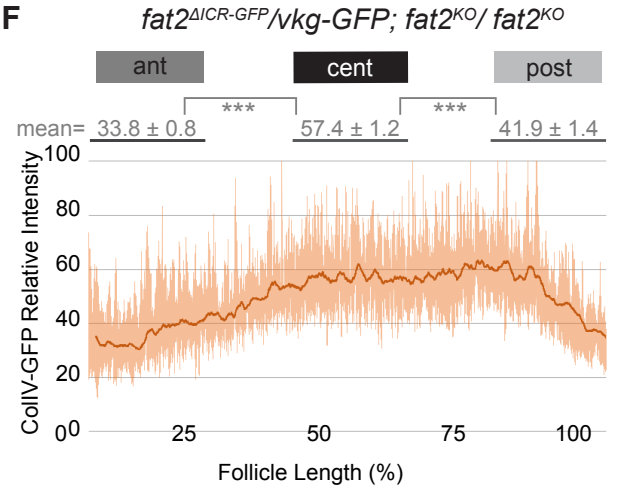

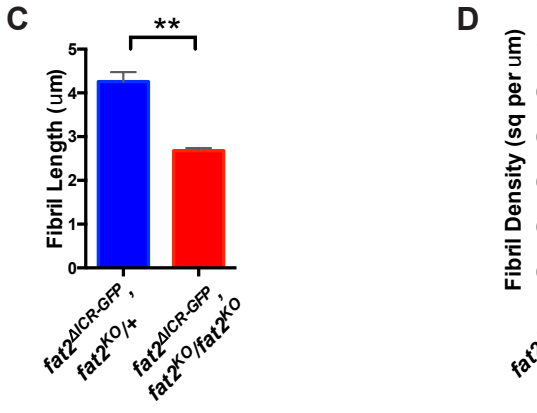

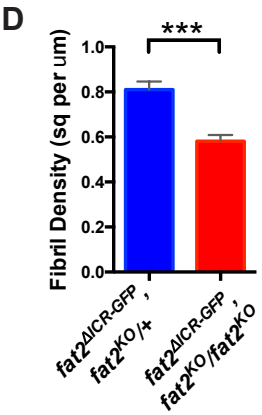

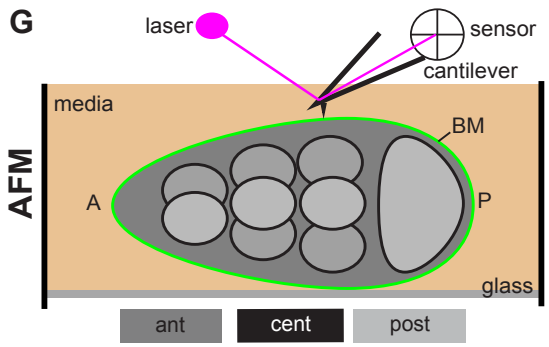

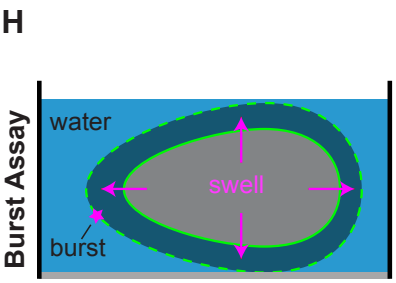

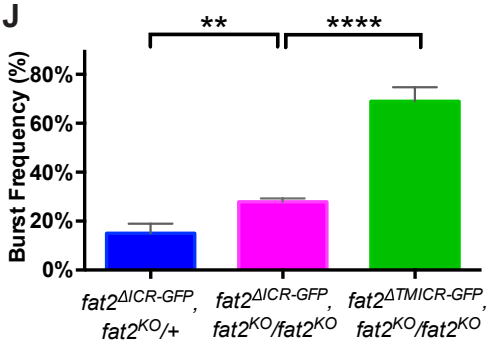

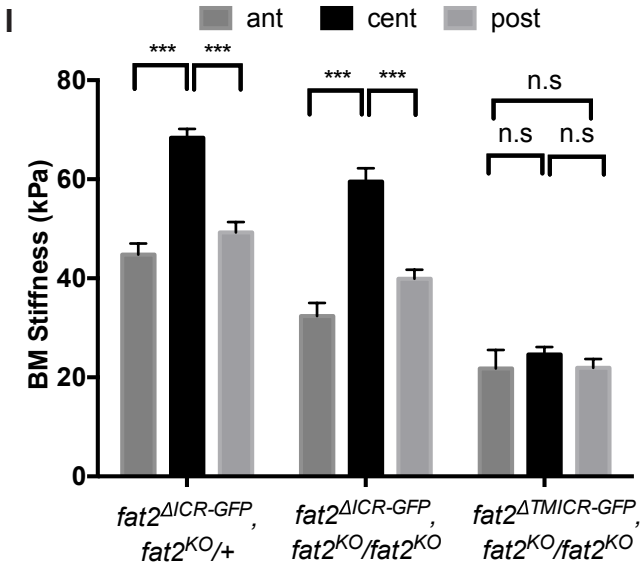

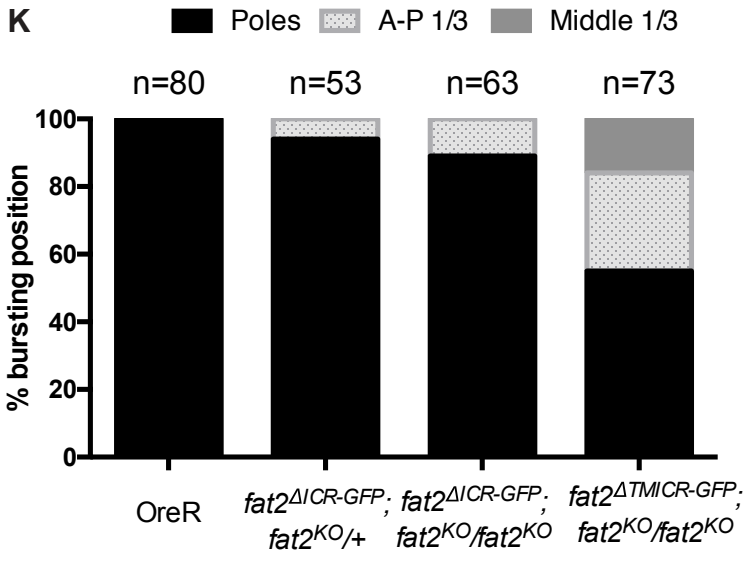

Fig.5

SUPPLEMENTAL EXPERIMENTAL PROCEDURES

Immunostaining and Imaging

Immunostaining and imaging were previously described (Chen et al., 2016). Antibodies used were listed in **KEY RESOURCE TABLE**.
Except for **Fig. S2C-E** with 100 μm scale bars, all scale bars are 10 μm.

in situ Larval Disc Wounding

Larvae carrying *5XQE-dsRed* (Zecca and Struhl, 2007) were used to visualize wing pouch *in situ* and *UAS-GFP-Vkg* is driven by *HmlΔ-Gal4* and *He-Gal4* (gifts from Katja Brückner). Third instar larvae were immobilized in ice-chilled PBS filled petri dish on ice. *in situ* wing pouch wounding was performed by holding the larva with one forcep while pinching the wing pouch with a dull tungsten needle. Larvae were transferred to a vial containing yeast paste to allow hemocyte migration and Vkg-GFP deposition to the basement membrane before fixation.

Image Analyses

ImSAnE was used to 'unroll' follicles as previously described (Chen et al., 2016; Heemskerk and Streichan, 2015). Cylinder projections from slices containing the basement membranes showing the full length of M-TRAIL were used for M-TRAIL quantification. Lengths of M-TRAIL were measured from ImSAnE-unrolled cylinder projection by Fiji. M-TRAIL migration percentages were calculated by dividing the M-TRAIL pixel length over the total pixel length of the D/V circumference. Angular velocity of rotation (ω) were calculated based on the percentage of follicle circumference covered by M-TRAIL, divided by the time post-heat shock minus M-TRAIL induction time. Data were analyzed and charts displayed using Prism 6 (GraphPad) and Excel (Microsoft). Figures were assembled by Illustrator CC 2017 (Adobe).

Biomechanical Assays

Basement membrane stiffness was measured by Atomic Force Microscopy (AFM), indenting live-cultured follicles 50 nm using a pyramidal tip cantilever as described previously (Crest et al., 2017). Young's Modulus of elasticity was calculated using a modified Hertz model; 4 measurements at each position were averaged for each data point.
For bursting assays, live follicles were first adhered to a poly-D lysine glass bottom dish (MatTek) in Schneider's media. Media was then replaced twice with distilled water and images were collected at 15 second intervals to identify time and site of follicle rupture, as described previously (Crest et al., 2017).

Fly Strains and Husbandry

Fly Strains used are listed in **KEY RESOURCE TABLE.** Fly strains were obtained from Bloomington Drosophila Stock Center except the following: *UAS-GFP-Vkg* and *UAS-GFP-Cg25c* are gifts from Stéphane Noselli (Van De Bor et al., 2015). *fat2*^{58D}*-FRT80, FRT42D-fat2-GFP, fat2*$^{\Delta ICR\text{-}GFP}$*, fat2*$^{\Delta TMICR\text{-}GFP}$ are gifts from Dr. Christian

Dahmann (Viktorinova et al., 2009) (Aurich and Dahmann, 2016). *UAS-SPARC-HA* is a gift from Eduardo Moreno (Portela et al., 2010). *vkg-GFP* and *trol-GFP* are from FlyTrap (Buszczak et al., 2007). *5xQE-DsRed* is a gift from Gary Struhl (Zecca and Struhl, 2007). *Act5C>CD2>Gal4, UAS-his2Av-mRFP* is a gift from Melanie Worley (Worley et al., 2013). Adult flies and larvae were maintained at 25°C. For ovaries samples, adult females were flipped onto fresh food daily for 1-2 days and were fed with yeast paste overnight before heat shock or dissection. Detailed genotypes in each figure are listed in **Table S1**.

KEY RESOURCES TABLE

REAGENT or RESOURCE	SOURCE	IDENTIFIER
Antibodies		
Mouse monoclonal Anti-GFP(3E6)	ThermoFisher	A11120
Rabbit HA-Tag mAb (C29F4)	Cell signaling	3724
Goat anti-Mouse IgG (H+L) Cross-Adsorbed Secondary Antibody, Alexa Fluor 488	ThermoFisher	A11001
Goat anti-Rabbit IgG (H+L) Cross-Adsorbed Secondary Antibody, Alexa Fluor 647	ThermoFisher	A21244
Donkey anti-Mouse IgG (H+L) Highly Cross-Adsorbed Secondary Antibody, Alexa Fluor 647	ThermoFisher	A31571
Chemicals		
FM4-64FX	ThermoFisher	F34653
Phalloidin-TRITC	Sigma	P1951
Alexa Fluor 647 Phalloidin	ThermoFisher	A22287
DAPI	Sigma	D9542
Experimental Model: *D. melanogaster*		
UAS-GFP-Vkg	Laboratory of Stéphane Noselli; (Van De Bor et al., 2015)	N/A
UAS-GFP-Cg25c	Laboratory of Stéphane Noselli; (Van De Bor et al., 2015)	N/A
$fat2^{KO}$	Laboratory of David Bilder: (“Organ sculpting by patterned extracellular matrix stiffness,” n.d.)	N/A
$fat2^{58D}$*-FRT80*	Laboratory of Christian Dahmann;(Viktorinova et al., 2009)	Flybase ID: FBal0241217
FRT42D-fat2-GFP	Laboratory of Christian Dahmann;(Viktorinova et al., 2009)	Flybase ID: FBal0241218
$fat2^{\Delta ICR\text{-}GFP}$	Laboratory of Christian Dahmann;(Aurich and Dahmann, 2016)	Flybase ID: FBal0319177
$fat2^{\Delta TMICR\text{-}GFP}$	Laboratory of Christian Dahmann;(Aurich and Dahmann, 2016)	Flybase ID: FBal0319178

P{UAS-SPARC.HA}	Laboratory of Eduardo Moreno; (Portela et al., 2010)	Flybase ID: FBtp0085610
HmlΔ-GAL4, UAS-GFP; He-GAL4	Laboratory of Katja Brückner	N/A
5xQE-DsRed	Laboratory of Gary Struhl	Flybase ID: FBtp0040071
P{GAL4-Act5C(FRT.CD2).P}S, P{UAS-His-RFP}3/TM3, Sb1	Laboratory of Iswar Hariharan; (Worley et al., 2013)	Flybase ID: FBst0051308
vkg-GFP	Flytrap; (Buszczak et al., 2007)	Flytrap ID: CC00791
trol-GFP	Flytrap; (Buszczak et al., 2007)	CA06698
w[1118]	Bloomington Drosophila Stock Center	Flybase ID: FBst0003605
P{ry[+t7.2]=hsFLP}22, w[*]	Bloomington Drosophila Stock Center	Flybase ID: FBst0008862
P{ry[+t7.2]=hsFLP}1, y[1] w[1118]; Dr[1]/TM3, Sb[1]	Bloomington Drosophila Stock Center	Flybase ID: FBst0026902
y1 w P{GAL4-Act5C(FRT.CD2).P}D*	Bloomington Drosophila Stock Center	Flybase ID: FBst0004779
P{w[+mC]=UAS-preproANF-EMD}136.3, y[1] w[*]	Bloomington Drosophila Stock Center	Flybase ID: FBst0007001
Software and Algorithms		
ImSAnE	(Heemskerk and Streichan, 2015)	N/A
Volocity	Perkin Elmer	N/A
Fiji	(Schindelin et al., 2012) http://fiji.sc/	N/A
Matlab 2015a	Mathworks	N/A
Prism V6	Graphpad	N/A
Illustrator CC 2017	Adobe	N/A
Excel	Microsoft	N/A

Table S1. Detailed Genotypes

Figure	Panel	Genotype
1	B	*hsFLP/+; UAS-GFP-Cg25c; Act5C >CD2>GAL4, UAS-His2Av-mRFP*
	D	*hsFLP/preproANF-EMD;;Act5C >CD2>GAL4, UAS-His2Av-mRFP*
	E	*hsFLP/+; UAS-GFP-Cg25c; Act5C >CD2>GAL4, UAS-His2Av-mRFP*
	F	*hsFLP/+; UAS-GFP-Cg25c; Act5C >CD2>GAL4, UAS-His2Av-mRFP*
	G	*hsFLP/+; UAS-GFP-Cg25c; Act5C >CD2>GAL4, UAS-His2Av-mRFP*
	H	*hsFLP/+; UAS-GFP-Cg25c; Act5C >CD2>GAL4, UAS-His2Av-mRFP*
	I	*hsFLP/+; UAS-GFP-Cg25c; Act5C >CD2>GAL4, UAS-His2Av-mRFP*
2	A	*hsFLP/+; UAS-GFP-Cg25c; Act5C >CD2>GAL4, UAS-His2Av-mRFP*
	B	*vkg-GFP*
	C	*yw,trol-GFP*
	D	*5xQE-DsRed/HmlΔ-GAL4, UAS-GFP; He-GAL4/ UAS-GFP-Vkg*
	E	*5xQE-DsRed/HmlΔ-GAL4, UAS-GFP; He-GAL4/ UAS-GFP-Vkg*
	F	*hsFLP/+; UAS-GFP-Cg25c; Act5C >CD2>GAL4, UAS-His2Av-mRFP, UAS-SPARC-HA*
3	B	*hsFLP/+; UAS-GFP-Cg25c; Act5C >CD2>GAL4, UAS-His2Av-mRFP*
	C	*hsFLP/+; UAS-GFP-Cg25c; Act5C >CD2>GAL4, UAS-His2Av-mRFP*
	D	*hsFLP/+; UAS-GFP-Cg25c; Act5C >CD2>GAL4, UAS-His2Av-mRFP*
	E	*hsFLP/+; UAS-GFP-Cg25c; UAS-GFP-vkg, Act5C >CD2>GAL4, UAS-GFP*
	F	*hsFLP/+; UAS-GFP-Cg25c; Act5C >CD2>GAL4, UAS-His2Av-mRFP*
4	A	*hsFLP/ Act5C >CD2>GAL4; UAS-GFP-Cg25c/+; $fat2^{KO}$ /+*
	B	*hsFLP/ Act5C >CD2>GAL4; UAS-GFP-Cg25c/+; $fat2^{KO}$ /$fat2^{KO}$*
	C	*hsFLP/ Act5C >CD2>GAL4; UAS-GFP-Cg25c/ $fat2^{\Delta ICR}$-GFP; $fat2^{KO}$ /$fat2^{KO}$*
	D	*hsFLP/ Act5C >CD2>GAL4; UAS-GFP-Cg25c/ $fat2^{\Delta TMICR}$-GFP; $fat2^{KO}$ /$fat2^{KO}$*
	E	*hsFLP/ Act5C >CD2>GAL4; UAS-GFP-Cg25c/ fat2-GFP; $fat2^{KO}$ /$fat2^{KO}$*
5	A	*vkg-GFP/ $fat2^{\Delta ICR}$-GFP; $fat2^{KO}$/ +*
	B	*vkg-GFP/ $fat2^{\Delta ICR}$-GFP; $fat2^{KO}$/ $fat2^{KO}$*
	E	*vkg-GFP/ $fat2^{\Delta ICR}$-GFP; $fat2^{KO}$/ +*
	F	*vkg-GFP/ $fat2^{\Delta ICR}$-GFP; $fat2^{KO}$/ $fat2^{KO}$*
Supp1	A	*hsFLP/+; UAS-GFP-Cg25c; Act5C >CD2>GAL4, UAS-His2Av-mRFP*
	B	*hsFLP/+; UAS-GFP-Cg25c; Act5C >CD2>GAL4, UAS-His2Av-mRFP*
	C	*Vkg-GFP*
	D	*hsFLP/+; UAS-GFP-Cg25c; Act5C >CD2>GAL4, UAS-His2Av-mRFP*
Supp2	A	*hsFLP/ Act5C >CD2>GAL4; UAS-GFP-Cg25c/+; $fat2^{58D}$-FRT80/$fat2^{KO}$*
	B	*hsFLP/ Act5C >CD2>GAL4; UAS-GFP-Cg25c/ $fat2^{\Delta ICR}$-GFP; $fat2^{KO}$ /$fat2^{KO}$*
	C	*$fat2^{KO}$/+*
	D	*$fat2^{KO}$/ $fat2^{KO}$*
	E	*$fat2^{\Delta ICR}$-GFP/+; $fat2^{KO}$/ $fat2^{KO}$*
	F	*hsFLP/ Act5C >CD2>GAL4; UAS-GFP-Cg25c/ $fat2^{\Delta ICR}$-GFP; $fat2^{58D}$-FRT80/+*
		hsFLP/ Act5C>CD2>GAL4; UAS-GFP-Cg25c/ $fat2^{\Delta ICR}$-GFP; $fat2^{58D}$-FRT80/$fat2^{KO}$

SUPPLEMENTAL FIGURE LEGENDS

Supplemental Figure 1

(A) Wing imaginal disc cells secrete M-TRAIL-derived GFP-Cg25c into the BM, as shown by GFP fluorescence and anti-GFP antibody staining under non-permeabilized conditions (white channel).

(B-D) Ubiquitous M-TRAIL-driven GFP-Cg25c does not alter follicle elongation at st. 10, compared to WT (OreR) or Vkg-GFP protein trap controls.

Supplemental Figure 2

(A) *fat2* anterior M-TRAIL clones show anterior accommodation (yellow and blue arrowheads).

(A') ImSAnE image of the same follicle.

(B) $fat2^{\Delta ICR}$ follicles, imaged via the membrane dye FM4-64FX, show no rotation throughout 90 minutes *ex vivo. Same 5 cells are labelled with yellow dots.*

(C-E) $fat2^{\Delta ICR}$ fosmid rescues egg elongation in $fat2^{KO}$ flies. Scale bars: 100μm.

(F) M-TRAIL reveals slowed but rotating follicles in $fat2^{\Delta ICR}$; $fat2^{58D}$/ $fat2^{KO}$ flies.

SUPPLEMENTAL REFERENCES

Aurich, F., Dahmann, C., 2016. A Mutation in fat2 Uncouples Tissue Elongation from Global Tissue Rotation. Cell Reports. doi:10.1016/j.celrep.2016.02.044

Buszczak, M., Paterno, S., Lighthouse, D., Bachman, J., Planck, J., Owen, S., Skora, A.D., Nystul, T.G., Ohlstein, B., Allen, A., Wilhelm, J.E., Murphy, T.D., Levis, R.W., Matunis, E., Srivali, N., Hoskins, R.A., Spradling, A.C., 2007. The carnegie protein trap library: a versatile tool for Drosophila developmental studies. Genetics 175, 1505–1531.

Chen, D.-Y., Lipari, K.R., Dehghan, Y., Streichan, S.J., Bilder, D., 2016. Symmetry Breaking in an Edgeless Epithelium by Fat2-Regulated Microtubule Polarity. Cell Reports 15, 1125–1133. doi:10.1016/j.celrep.2016.04.014

Crest, J., Diz-Munoz, A., Chen, D.-Y., Fletcher, D.A., Bilder, D., 2017. Organ sculpting by patterned extracellular matrix stiffness. eLife 6, e24958. doi:10.7554/eLife.24958

Heemskerk, I., Streichan, S.J., 2015. Tissue cartography: compressing bio-image data by dimensional reduction. Nature Methods 12, 1139–1142.

Organ sculpting by patterned extracellular matrix stiffness, n.d. Organ sculpting by patterned extracellular matrix stiffness.

Portela, M., Casas-Tinto, S., Rhiner, C., López-Gay, J.M., Domínguez, O., Soldini, D., Moreno, E., 2010. Drosophila SPARC is a self-protective signal expressed by loser cells during cell competition. Dev Cell 19, 562–573. doi:10.1016/j.devcel.2010.09.004

Schindelin, J., Arganda-Carreras, I., Frise, E., Kaynig, V., Longair, M., Pietzsch, T., Preibisch, S., Rueden, C., Saalfeld, S., Schmid, B., Tinevez, J.-Y., White, D.J., Hartenstein, V., Eliceiri, K., Tomancak, P., Cardona, A., 2012. Fiji: an open-source platform for biological-image analysis. Nat. Methods 9, 676–682. doi:10.1038/nmeth.2019

Van De Bor, V., Zimniak, G., Papone, L., Cerezo, D., Malbouyres, M., Juan, T.,

Ruggiero, F., Noselli, S., 2015. Companion Blood Cells Control Ovarian Stem Cell Niche Microenvironment and Homeostasis. Cell Reports 13, 546–560. doi:10.1016/j.celrep.2015.09.008

Viktorinova, I., Konig, T., Schlichting, K., Dahmann, C., 2009. The cadherin Fat2 is required for planar cell polarity in the Drosophila ovary. Development 136, 4123–4132. doi:10.1242/dev.039099

Worley, M.I., Setiawan, L., Hariharan, I.K., 2013. TIE-DYE: a combinatorial marking system to visualize and genetically manipulate clones during development in Drosophila melanogaster. Development 140, 3275–3284. doi:10.1242/dev.096057

Zecca, M., Struhl, G., 2007. Recruitment of cells into the Drosophila wing primordium by a feed-forward circuit of vestigial autoregulation. Development 134, 3001–3010. doi:10.1242/dev.006411

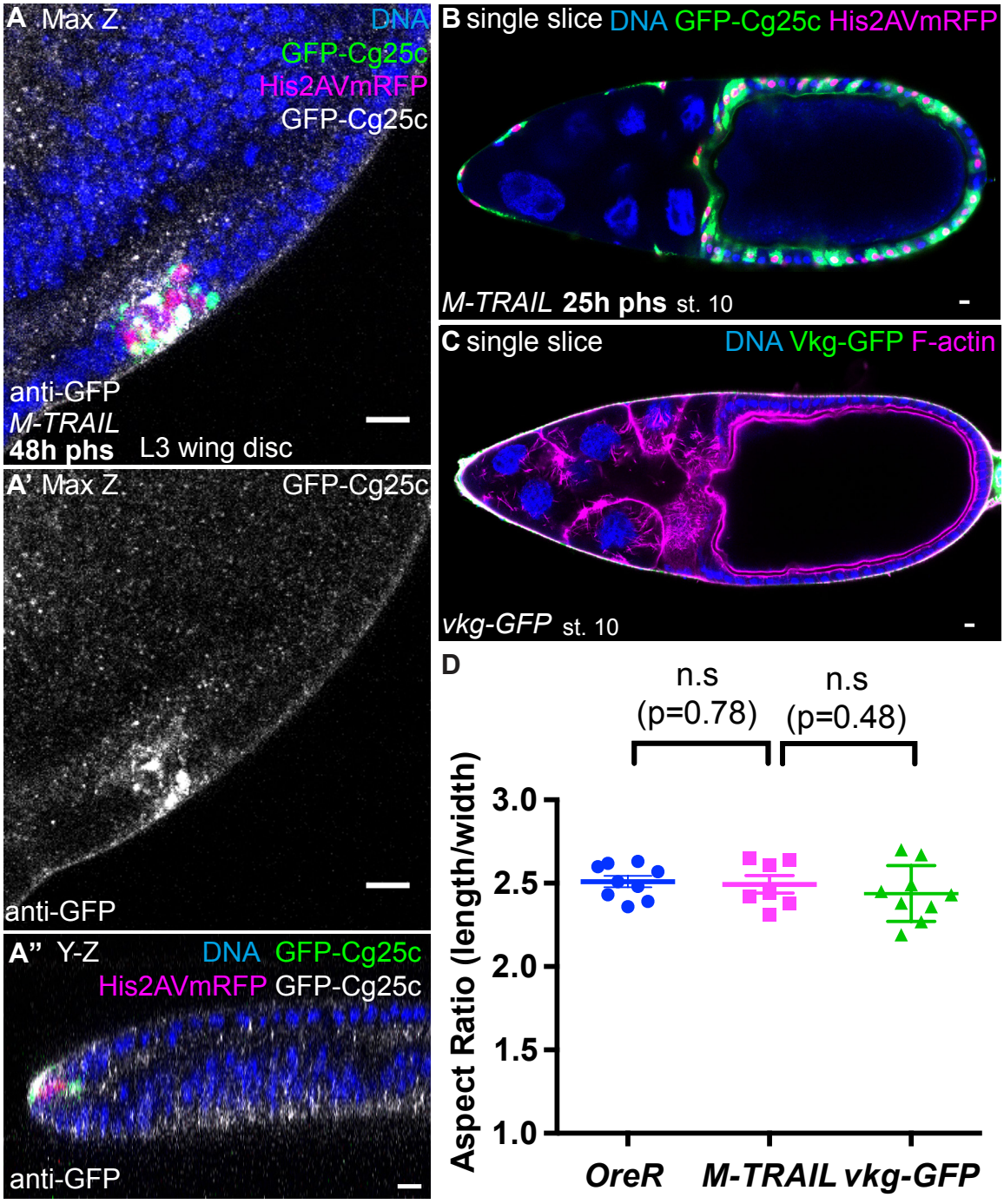

Supplemental Figure 1

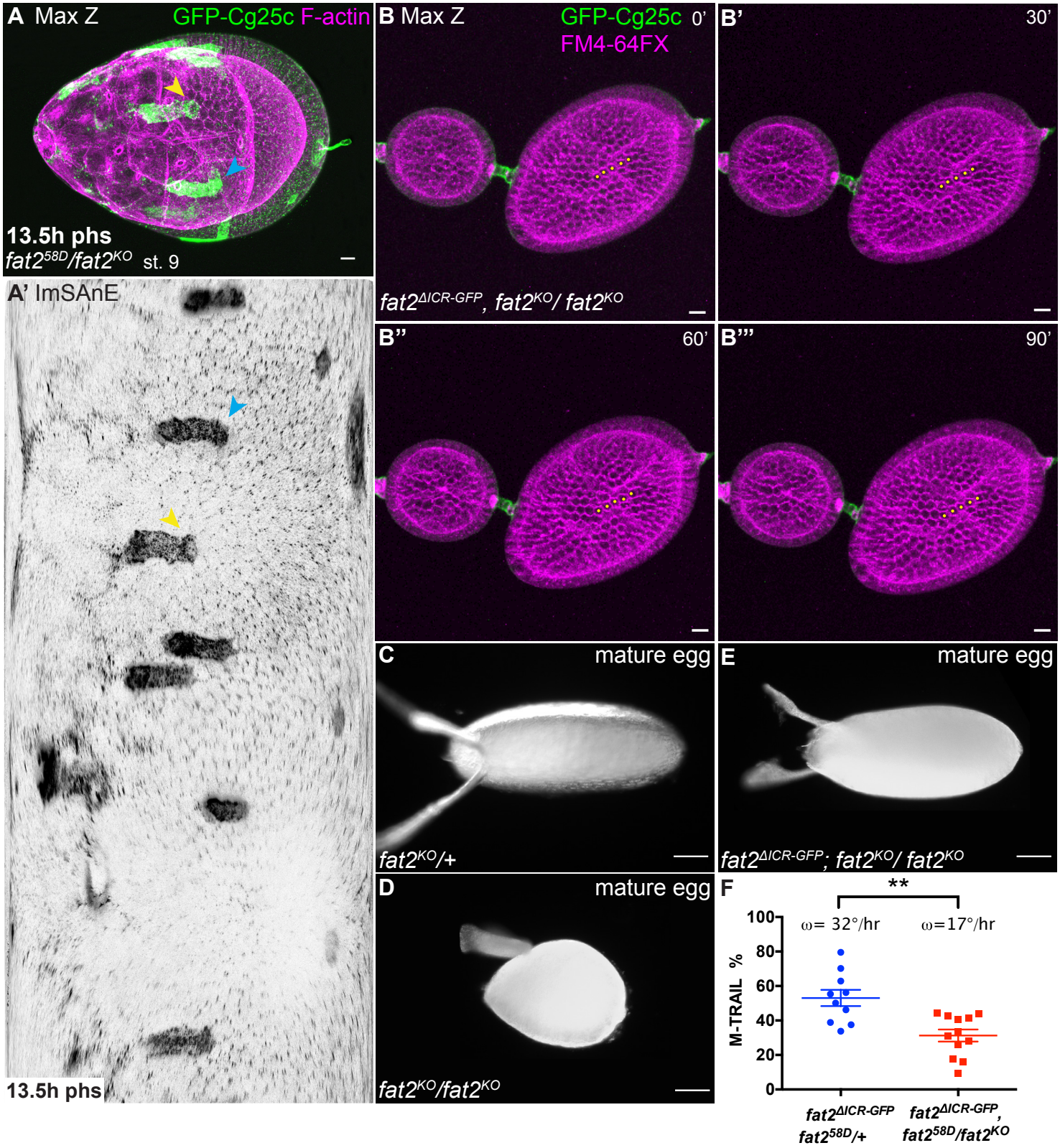

Supplemental Figure 2